isvr Institute of Sound and Vibration Research

Performance Evaluation of a Feedback Active Isolation System with Inertial Actuators

S.J. Elliott, P. Gardonio, B. Rafaely, R. Harris and K. Heron

ISVR Technical Memorandum 832

December 1998

University of Southampton

SCIENTIFIC PUBLICATIONS BY THE ISVR

Technical Reports are published to promote timely dissemination of research results by ISVR personnel. This medium permits more detailed presentation than is usually acceptable for scientific journals. Responsibility for both the content and any opinions expressed rests entirely with the author(s).

Technical Memoranda are produced to enable the early or preliminary release of information by ISVR personnel where such release is deemed to the appropriate. Information contained in these memoranda may be incomplete, or form part of a continuing programme; this should be borne in mind when using or quoting from these documents.

Contract Reports are produced to record the results of scientific work carried out for sponsors, under contract. The ISVR treats these reports as confidential to sponsors and does not make them available for general circulation. Individual sponsors may, however, authorize subsequent release of the material.

UNIVERSITY OF SOUTHAMPTON

INSTITUTE OF SOUND AND VIBRATION RESEARCH

SIGNAL PROCESSING & CONTROL GROUP

Performance Evaluation of a Feedback Active Isolation System with Inertial Actuators

by

S J Elliott, P Gardonio and B Rafaely, ISVR
R Harris and K Heron, DERA, Farnborough, Hampshire

ISVR Technical Memorandum No. 832

December 1998

Authorised for issue by
Prof S J Elliott
Group Chairman

Acknowledgement

The work reported in this memorandum was supported by the Aero-Structures Department at DERA Farnborough under the DTI funded project "Active Isolator Research for Aircraft Trim Panels" (AIRAT).

CONTENTS:

LIST OF FIGURES

1. INTRODUCTION

This report describes the design and performance of a feedback controller for the active isolation of vibration transmitted from one plate to another through flexible mounts. The construction and testing of the inertial actuators used as secondary sources is described first, followed by a discussion of the response from the actuator input to sensor output on the plate system. This 'plant' response constitutes the system under control by the feedback system and the way in which it behaves, particularly in relation to its phase response, will determine the performance limitations of the feedback system. The performance of the feedback controller is then predicted and these predictions compared with the experimental results for a single active mount.

The experimental arrangement for a multichannel system which has three active mounts is then described. The theory of multichannel feedback control is briefly reviewed and then the additional constraints on stability and performance introduced by the coupling between the mounts are discussed.

2. DESIGN AND TESTING OF THE INERTIAL ACTUATOR

The inertial actuator design is shown in Figure 2.1 and consists of a case with a loudspeaker coil rigidly attached to it, with a moving magnet suspended on a rubber diaphragm within the case. The magnet thus acts as both the inertial mass and generates the magnetic field required for electromagnetic actuation. An accelerometer is also built into the actuator.

The mass of the magnet assembly is about 77 gms and that of the total actuator is about 137 gms. The measured force output of the actuator when driven by a constant

current amplifier and mounted on a large rigid mass is shown in Figure 2.2 which shows the expected second order behaviour, with a constant force output above the fundamental resonance frequency of about 70 Hz. The phase of the output force per unit input voltage is also close to 0° above this frequency, indicating that the actuator is acting almost like an ideal device in this frequency range. Notice, however, that at low frequencies, below the natural frequency, the phase rises by 180°, which indicates that the electromagnetic force is predominantly overcoming the stiffness of the suspension to move the mass and so the inertial force generated by the mass is out of phase with the driving force. The origin of the additional peak at about 4.5 kHz seen in Figure 2.2 is unknown, but since it does not appear in any of the subsequent plots, for which the force gauge was not used, it is assumed to be an artefact of the force measurement.

The stiffness of the suspension inside the actuator (K_S) can be simply calculated from the moving mass ($M = 77$g) and the natural frequency (f_0) since they are related by

$$2\pi f_0 = \sqrt{\frac{K_S}{M}} \tag{2.1}$$

from which the stiffness can be calculated to be about 15,000 $N\,m^{-1}$ or 15 $N\,mm^{-1}$. The damping ratio of the 70 Hz resonance in Figure 2.2 is about $\zeta_{mount} = 0.15$ which would be caused by a viscous damper having a resistance of about $C_s = 10\ N\,m^{-1}$s in parallel with the spring.

The resistance and inductance of the coil in the inertial actuator were about $R = 4\Omega$ and $L = 0.06$mH, but since a constant current amplifier was used to drive the actuator, the secondary force, F_S, is assumed to be directly proportional to the input voltage, V_{in}.

A simple second order model of the inertial actuator is shown in Figure 2.3 from which the ratio of the force transmitted to the rigid base, F_A, to the secondary force, F_S, can be derived as being

$$\frac{F_A}{F_S} = \frac{\omega^2 M}{K - \omega^2 M} = T_A(j\omega) \tag{2.2}$$

where M is the moving mass and K is the complex stiffness of the suspension which is equal to $K_s + j\omega C_c$, and $T_A(j\omega)$ can be termed the actuator response, which is used below

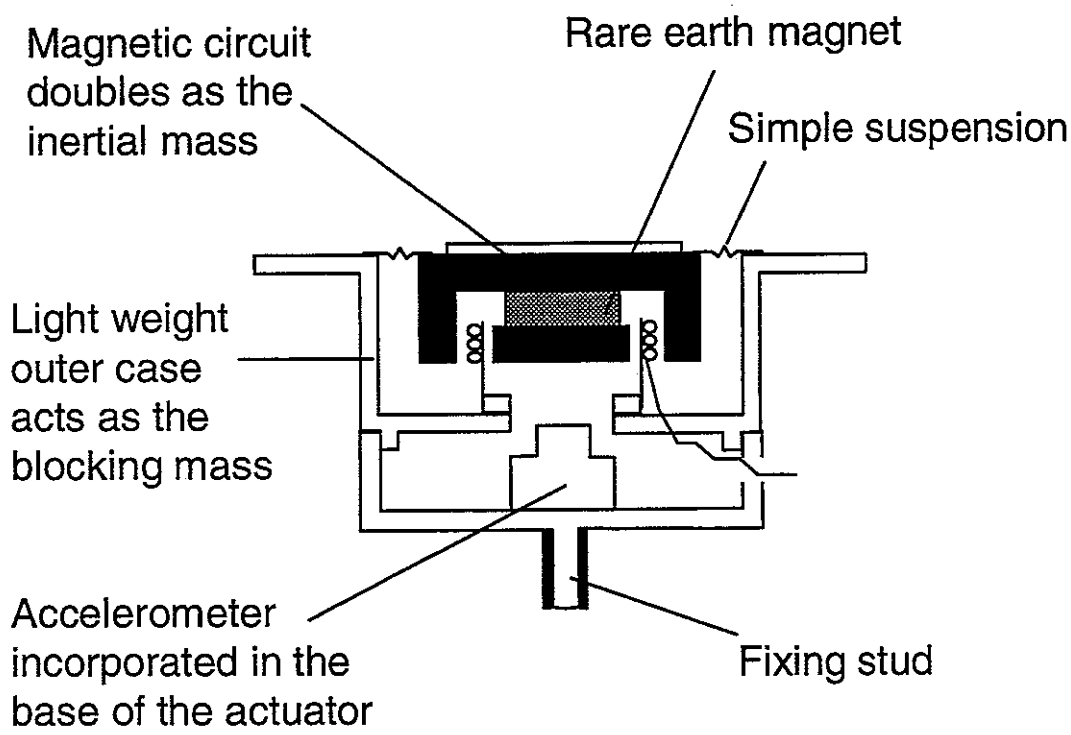

Figure 2.1 Sketch of the internal design of the inertial actuator

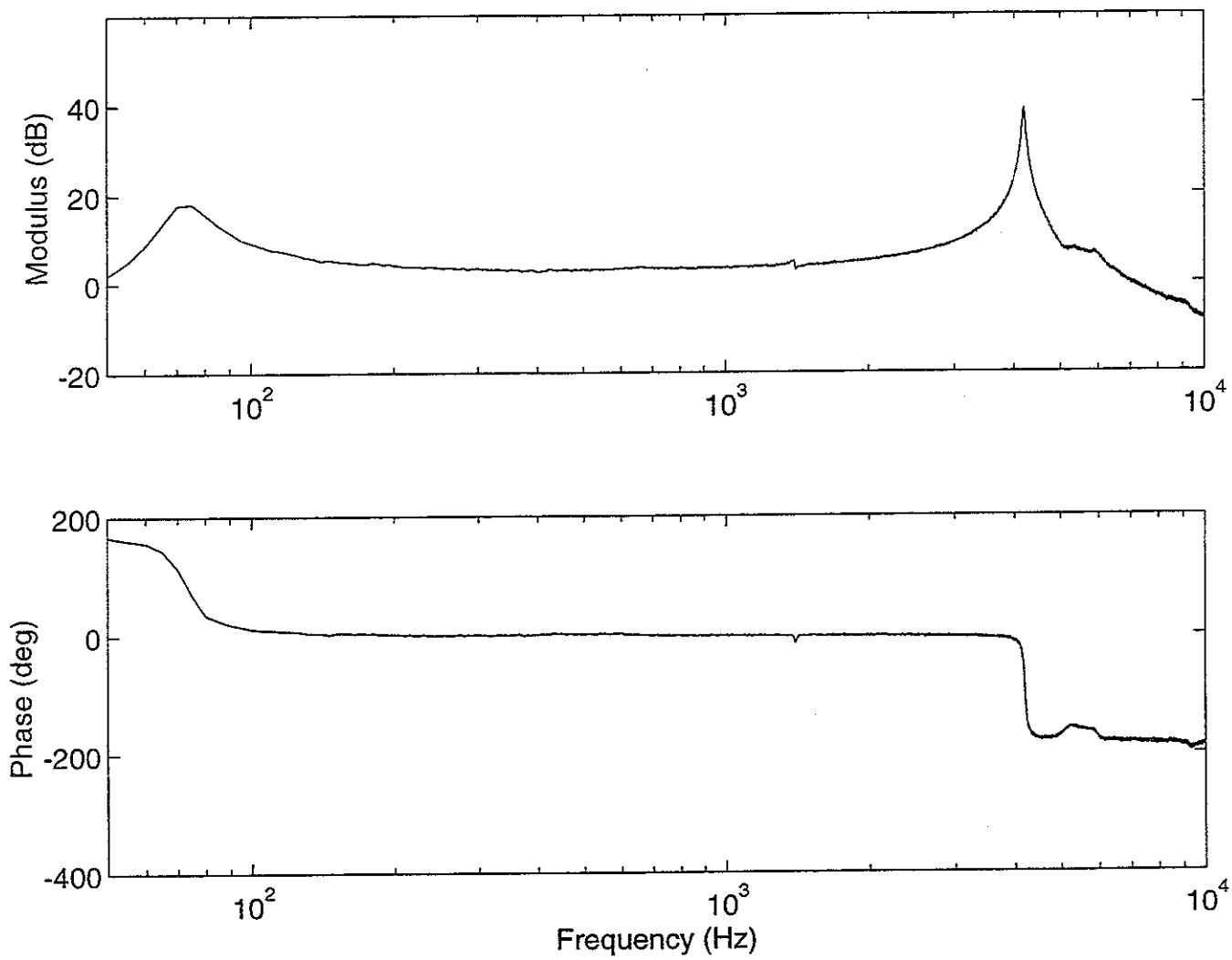

Figure 2.2 Amplitude and phase of the measured frequency response of the output force from the inertial actuator per unit input voltage when mount on a rigid base.

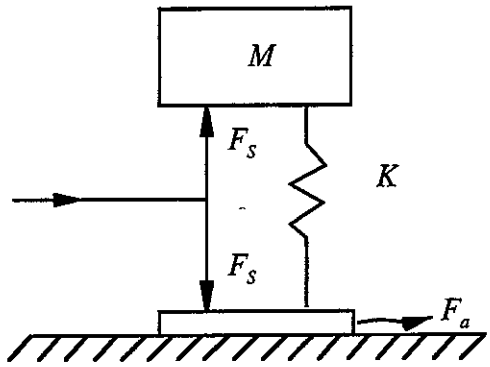

Figure 2.3 Second order model of the moving parts of the actuator which is mounted on a rigid base and is being driven by an input signal to produce a secondary force of F_s, which then generates a total actuator force onto the rigid base of F_a.

3. BEHAVIOUR OF THE ACTUATOR AND THE PASSIVE MOUNT ON A RIGID BASE

An important step towards understanding the frequency response of the complete experimental system is to study the response of the inertial actuator when mounted on the passive mount placed on a rigid base. A simple two degree of freedom model for this system is shown in Figure 3.1. The moving mass of the inertial actuator is M_2 (77 g), the stiffness of the actuator suspension is K_2 (15 $N\,mm^{-1}$), the mass of the actuator body and mounting components is M_1 (59 g) and the stiffness of the passive mount was K_1 (90 $N\,mm^{-1}$). The equations of motion for the two degree of freedom model of the actuator lead to the coupled set of equations for the complex V_1 and V_2 in terms of F_S as

$$\begin{bmatrix} j\omega M_1 + \frac{K_1+K_2}{j\omega} & -\frac{K_2}{j\omega} \\ -\frac{K_2}{j\omega} & j\omega M_2 + \frac{K_2}{j\omega} \end{bmatrix} \begin{bmatrix} V_1 \\ V_2 \end{bmatrix} = \begin{bmatrix} -F_S \\ F_S \end{bmatrix}, \tag{3.1}$$

in which the complex stiffnesses K_1 and K_2 contain the damping terms, from which V_1 and V_2 can be calculated as a function of F_S. The measured frequency response between the actuator input and the velocity on top of the passive mount (V_1) is shown in 3.2(a) and that calculated using equation (3.1) are shown in Figure 3.3, which also shows the behaviour of V_2 (faint line).

Although at each of the natural frequencies of the second order system both masses are moving, at the first resonance the motion of M_2 is considerably larger than M_1 as shown in Figure 3.3. This first resonance can thus be strongly associated with the actuator and occurs at a similar frequency to the natural frequency of the actuator alone when mounted on a rigid base. At the second resonance both masses move in phase, but that of M_2 is considerably smaller than that of M_1 because it is decoupled by the actuator suspension and so this resonance can be strongly associated with that of the passive mount. Further simplification of the dynamics is suggested by the fact that the two resonances of the two degree of freedom system can be reasonably well associated with the dynamics of either the actuator or the mount alone.

When the actuator is mounted on a flexible structure, such as the passive mount, so that it generates a velocity V_1, the force applied by the actuator can be written as

$$F_A = T_A(j\omega)F_S - Z_A(j\omega)V_1 \tag{3.2}$$

where $T_A(j\omega)$ is the ratio of F_A/F_S if $V_1 = 0$, i.e. it is mounted on a rigid base (as given by equation (2.1)) and $Z_A(j\omega)$ is the mechanical input impedance to the actuator from the base looking upwards. The velocity of the mount structure in response to an input force of F_a can be written as

$$V_1 = M_S(j\omega)F_A \tag{3.3}$$

where $M_S(j\omega)$ is the input mobility of passive mount in this case at the actuator mounting point. Substituting (3.3) into (3.2) we obtain

$$F_A = \left[1 + Z_A(j\omega) M_S(j\omega)\right]^{-1} T_A(j\omega) F_S \tag{3.4}$$

and so the velocity at the top of the passive mount per unit secondary force is equal to

$$V_1/F_S = \left[1 + Z_A(j\omega) M_S(j\omega)\right]^{-1} T_A(j\omega) M_S(j\omega) \, . \tag{3.5}$$

Figure 3.4 shows a block diagram of this mechanical interaction, together with the electrical feedback control discussed below.

If the product of the actuator's mechanical input impedance and the structure's mechanical input mobility is much less than unity, then the force applied by the actuator is almost the same as if it were mounted on a rigid base, i.e.

$$\text{if} \quad Z_A(j\omega) M_S(j\omega) \ll 1 \quad , \quad \text{then} \quad F_A \approx T_A(j\omega) F_S \, . \tag{3.6, 3.7}$$

So for the specific case considered above, the condition given by (3.6) is reasonably true above the resonant frequency of the actuator.

When the actuator dynamics are reasonably well decoupled from those of the structure to which they are attached, then the overall response of the structure to the secondary actuator can be written as

$$\frac{V_1}{F_S} = T_A(j\omega) \, M_S(j\omega) \, . \tag{3.8}$$

Since in this case $T_A(j\omega)$ is given by equation (2.1) as

$$T_A(j\omega) = \frac{\omega^2 M_2}{K_2 - \omega^2 M_2} \tag{3.9}$$

and the input mobility of the mass M_1 and passive mount of stiffness K_1 is equal to

$$M_M(j\omega) = \frac{j\omega}{K_1 - \omega^2 M_1}, \tag{3.10}$$

which is equal to $M_S(j\omega)$ in this case, the approximation to the overall response given by equation (3.8) can be directly calculated, and is compared with that generated by the complete equation for this response (3.1) in Figure 3.5.

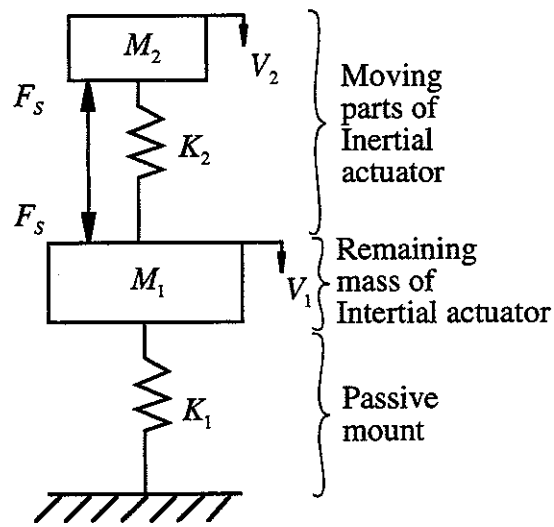

Figure 3.1 Two degree of freedom model for the inertial actuator (M_2, K_2), driven by the electromagnetic force F_S, generating a velocity V_1 on the actuator body (M_1) which is mounted on the passive mount (K_1) and the velocity V_2 on the actuator mass.

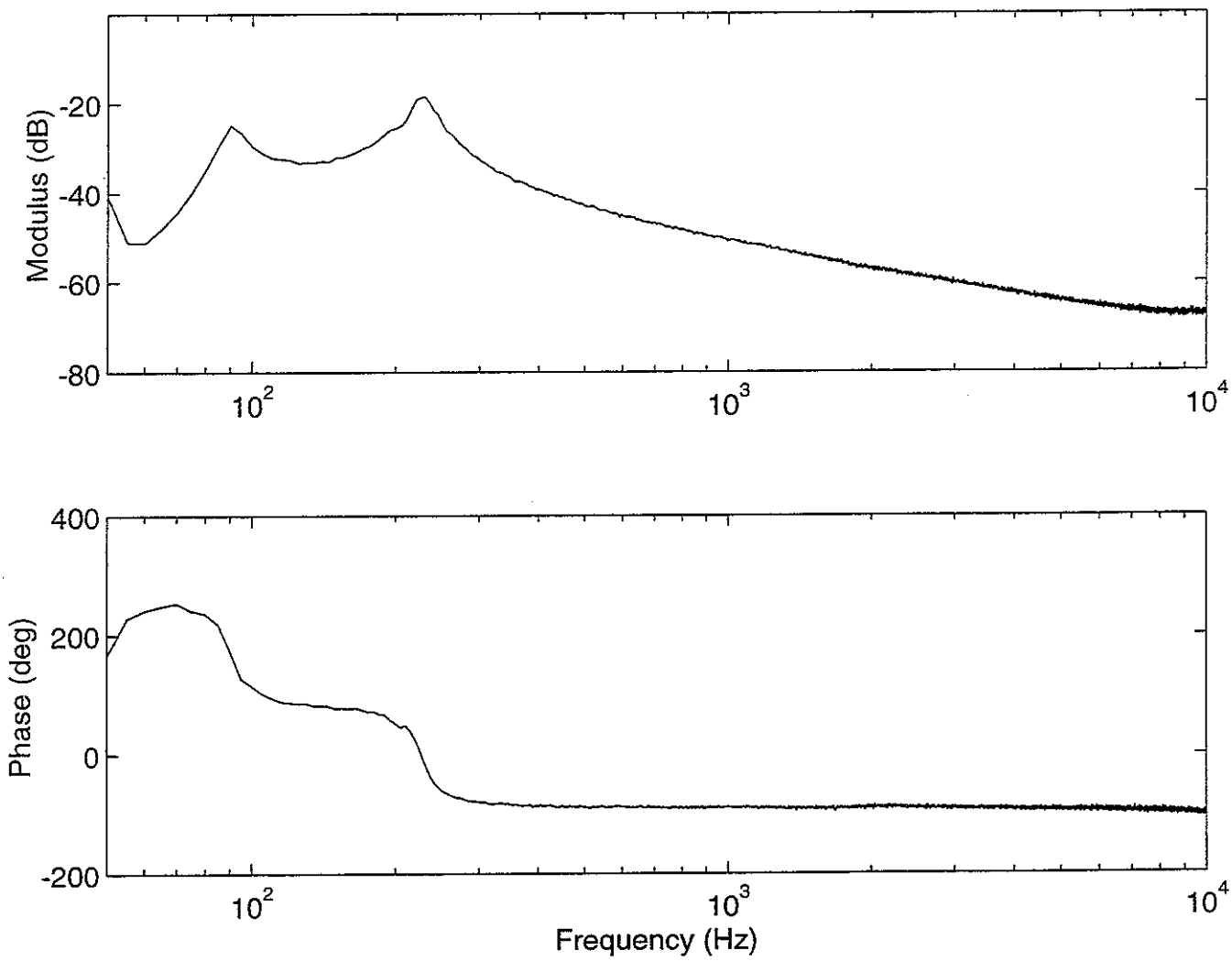

Figure 3.2 Measured frequency response of the velocity at the top of the passive mount per unit input secondary signal to the intertial actuator when the passive mount is mounted on a rigid base.

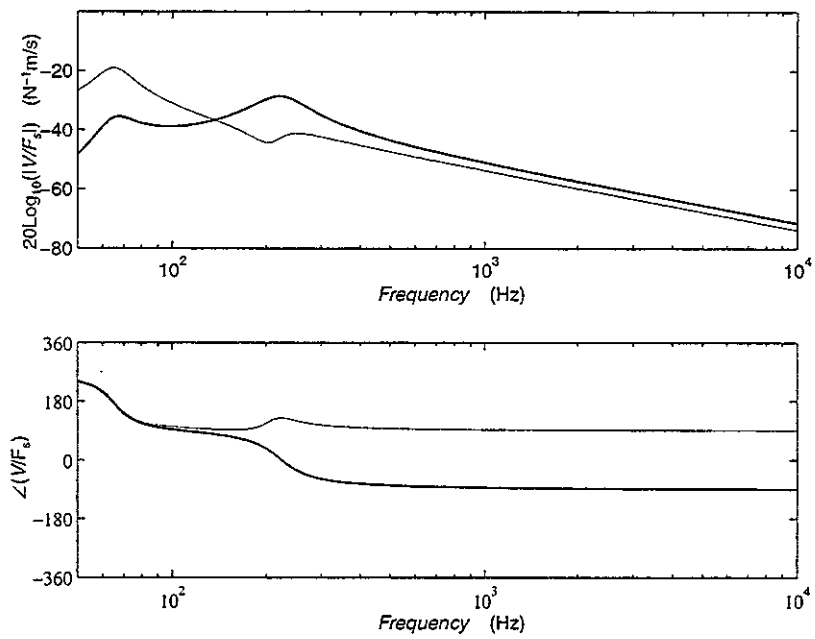

Figure 3.3 Modulus and phase of the velocity on the top of the passive mount (solid line, V_1), compared with that on the moving mass of the actuator (faint line, V_2) calculated from the two degree of freedom model.

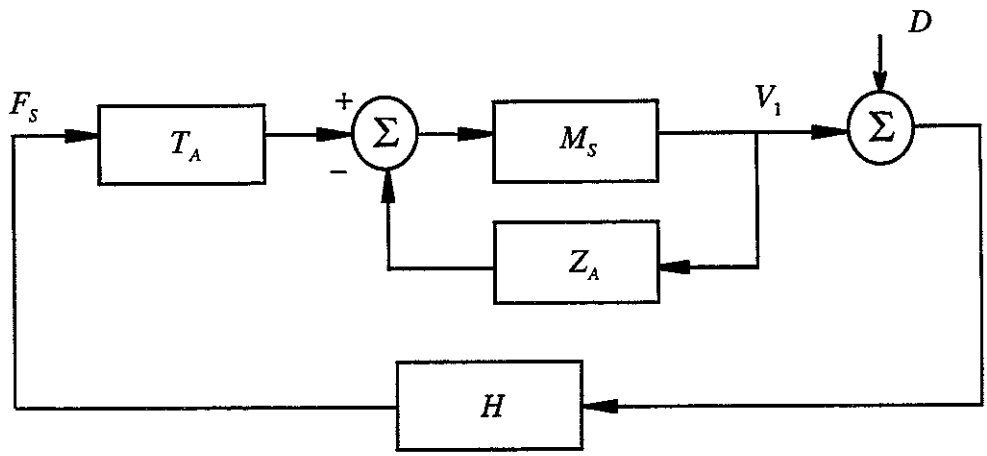

Figure 3.4 Block diagram of the mechanical interaction between the actuator, with blocked transfer function T_A and internal mechanical impedance Z_A, and the structure being controlled, with mobility M_S, together with the electrical feedback controller, H.

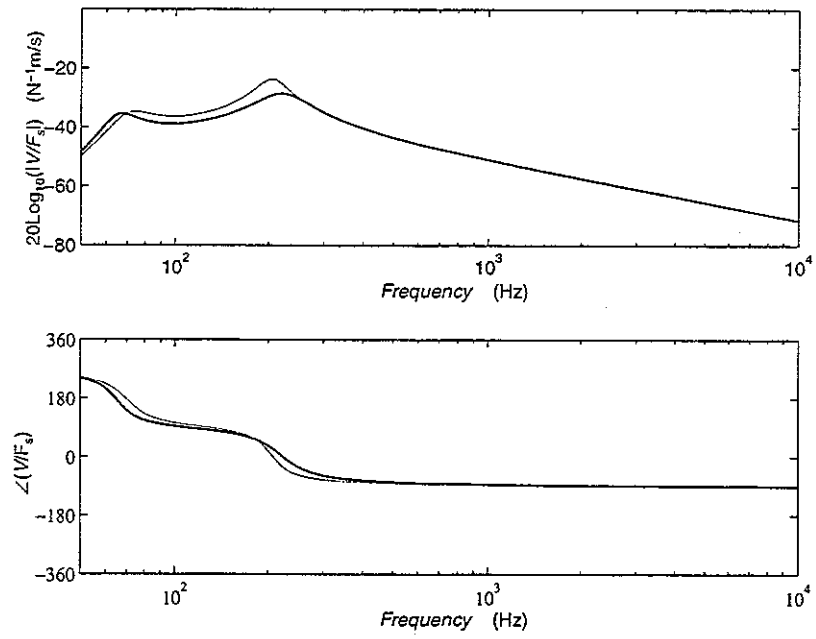

Figure 3.5 Modulus and phase of the velocity at the top of the passive mount per unit secondary force calculated using the exact expression, equation (3.1) (solid line) and equation (3.8) which assumes that the actuator and mount dynamics are uncoupled (faint line).

4. EXPERIMENTAL ARRANGEMENT AND COMPLETE PLANT RESPONSE

An initial estimate of the final plant response was obtained by placing a plate between the actuator and passive mount, and the measured frequency response of this system from actuator input to integrated accelerometer output is shown in Figure 4.1.

Figure 4.2 shows the final experimental arrangement in which an *I* beam driven by the primary source is coupled to a receiver plate via three passive mounts each with an inertial actuator and accelerometer above them for active control.

A simple model for a single mount in this arrangement is shown in Figure 4.3 in which the *I* beam is assumed to have a much lower mobility than the other

components and are thus approximated as a rigid base. The input mobility of the complete structure, as seen by the actuator is now

$$M_S(j\omega) = \frac{M_P(j\omega)M_M(j\omega)}{M_P(j\omega)+M_M(j\omega)} \tag{4.1}$$

where $M_P(j\omega)$ is the input mobility of the plate, $M_M(j\omega)$ is the input mobility of the remaining mass of the actuator and passive mount as given by equation (3.10).

Figure 4.3 shows the calculated input mobility to the complete structure, $M_S(j\omega)$, compared with that of the mount alone, $M_M(j\omega)$ and of the plate, which was assumed to be 0.75mm aluminium of dimensions 720 x 550mm attached near the centre of plate. Notice how the phase of $M_S(j\omega)$ must again be between $\pm 90°$ since the system is entirely passive.

Figure 4.4 shows the complete response from secondary force to velocity at the top of the mount calculated from the simplified model for $M_S(j\omega)$ and using equation (3.8) as the approximation for the complete response which assumes no coupling and equation (3.10) for the actuator response. The measured response from actuator input voltage to output velocity, as measured with an accelerometer, is shown in Figure 4.5

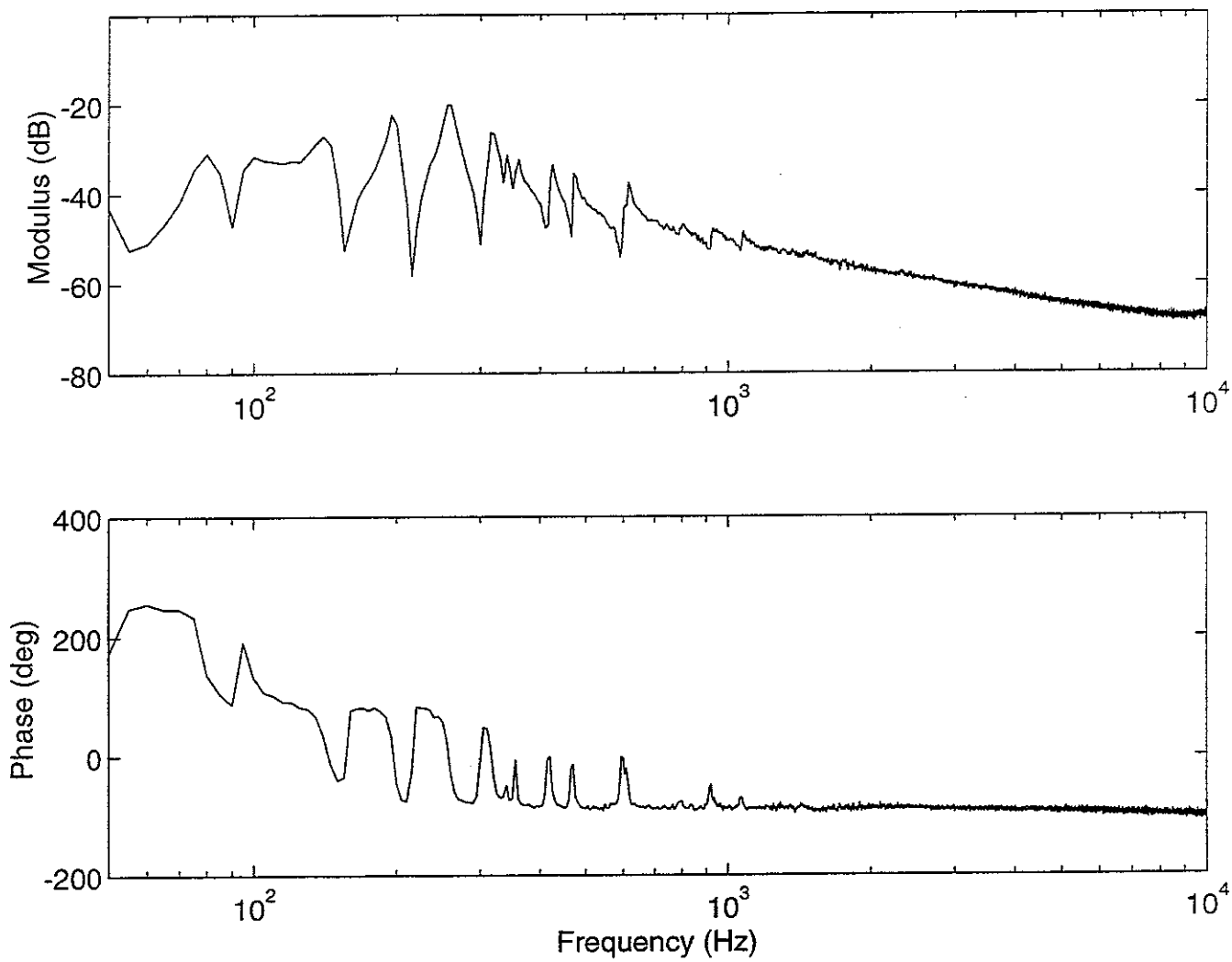

Figure 4.1 Frequency response from initial experiments with a plate placed between the inertial actuator and passive mount.

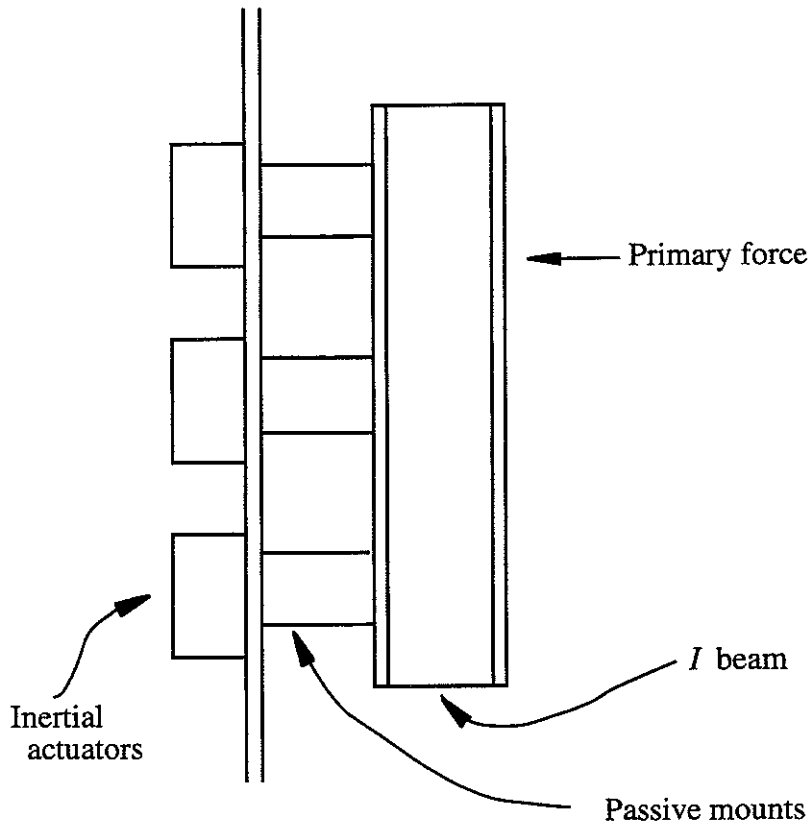

Figure 4.2 Sketch of the final experimental arrangement with an I beam driven by the primary force coupled to a receiver plate via three actively controlled passive mounts.

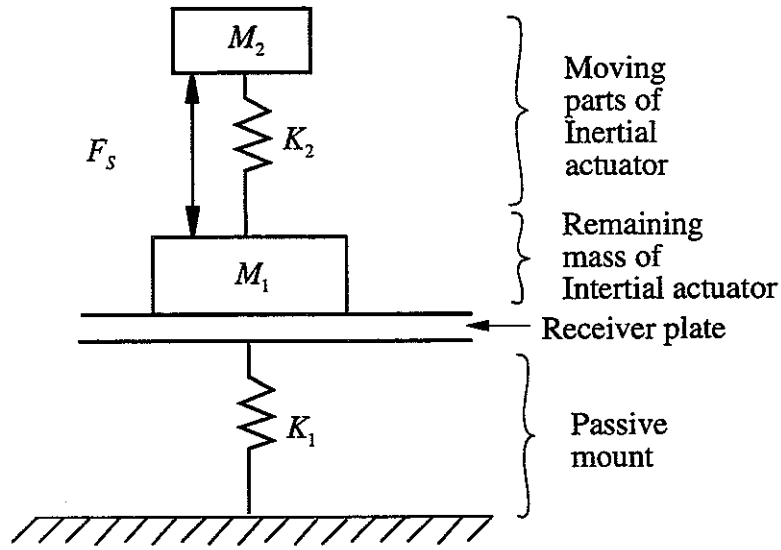

Figure 4.3 Simple model of the arrangement used in the experiments, in which the I beam is assumed to act as a rigid base.

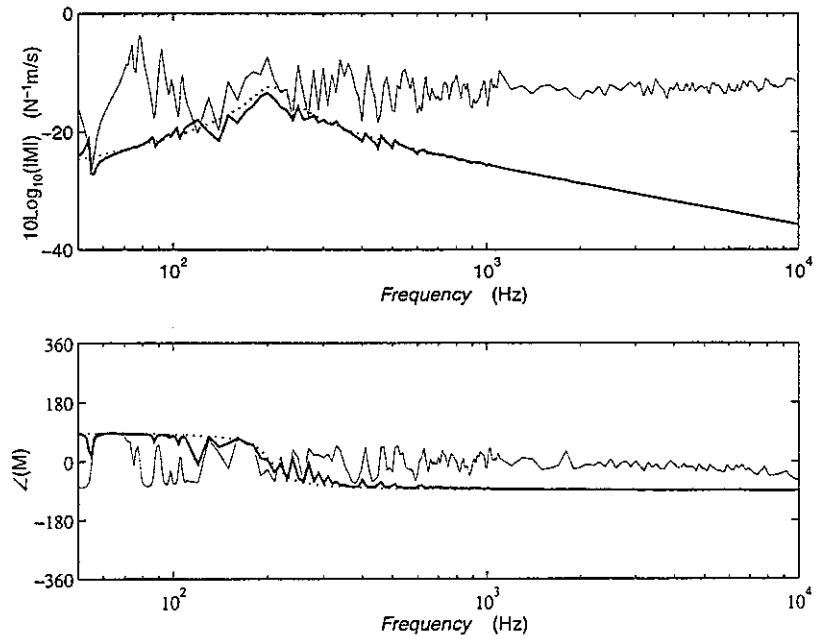

Figure 4.4 The calculated input mobility as seen by the inertial actuator for the model shown in Figure 4.3 (solid line) and that of the passive mount alone (dotted line) and that of the plate alone (faint line).

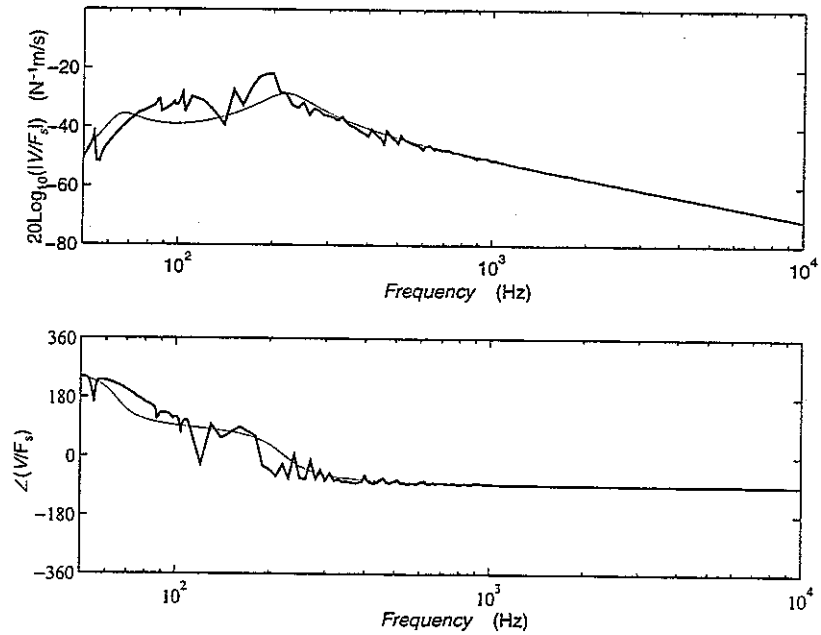

Figure 4.5 The complete response from secondary force to velocity on top of the mount calculated using the model of Figure 4.3 (solid line) and the same without the receiver plate (faint line).

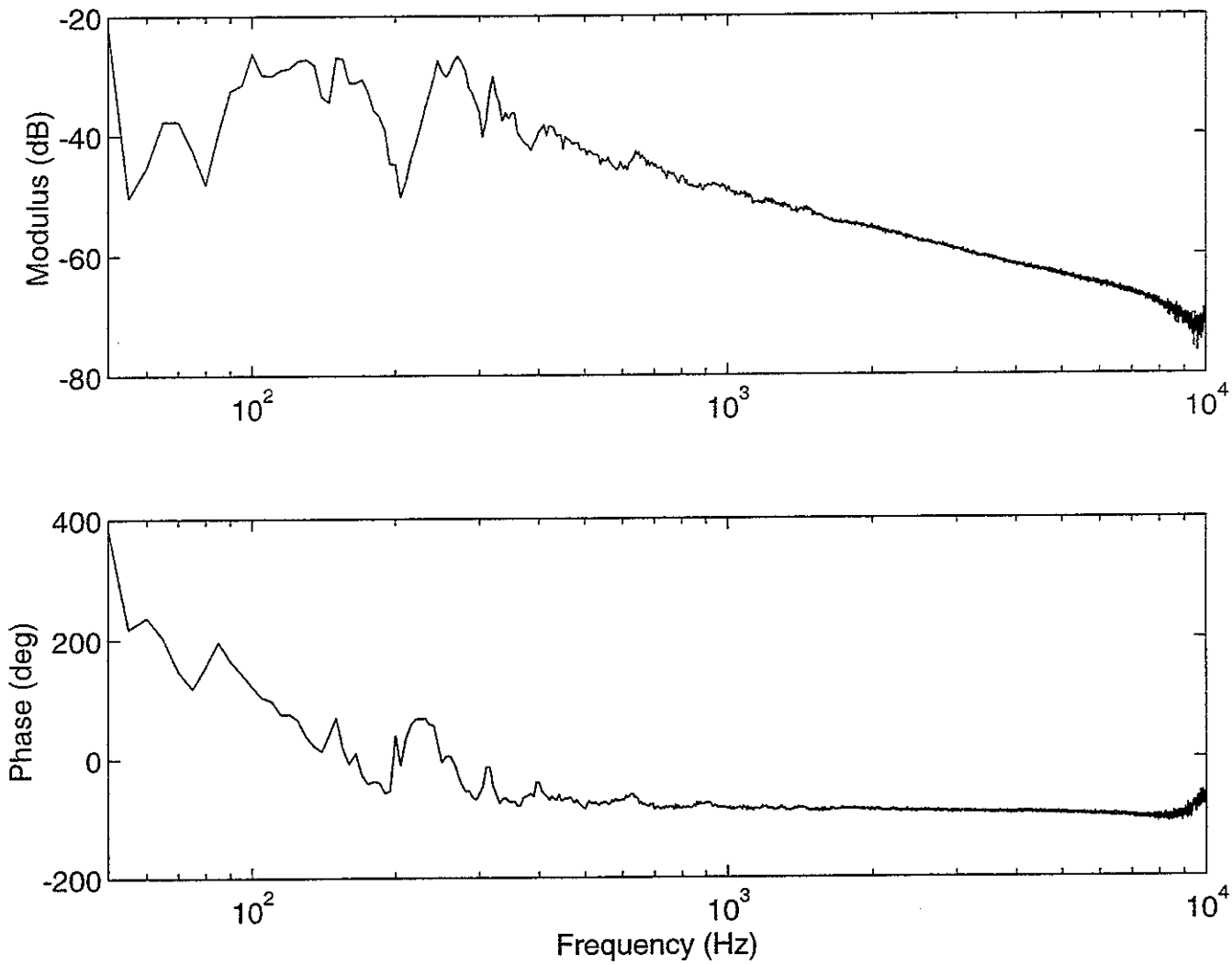

Figure 4.6 The measured response from actuator input signal to integrated accelerometer output signal for a single channel of the final experimental system shown in Figure 4.1.

5. SINGLE CHANNEL FEEDBACK CONTROL DESIGN AND PERFORMANCE

The complete transfer response from the actuator input to sensor output is referred to as the 'plant' response and its transfer function is denoted $G(s)$. The vibration due to the primary shaker acts as a "disturbance" at the sensor output and is denoted $D(s)$ in Figure 5.1 which also shows the sensor output being fed back to the actuator input via a negative feedback controller with transfer function - $H(s)$. The sensitivity function of the feedback controller is given by the ratio of the controlled to uncontrolled output of the plant (Franklin *et al*, 1994), and is equal to

$$S(s) = \frac{E(s)}{D(s)} = \frac{1}{1+G(s)H(s)} . \tag{5.1}$$

The closed loop system is only stable if its poles, which are given by the roots of the characteristic equation,

$$1+G(s)H(s) = 0 \tag{5.2}$$

are in the right hand half of the s plane. In practice closed loop stability can be assessed from the open loop frequency response, $G(j\omega)H(j\omega)$, which is itself assumed to be stable, by plotting this in a polar diagram and checking whether this plot encloses the Nyquist point, –1, 0, as ω varies from $-\infty$ to ∞. Assuming the feedback controller is a fixed gain, the resulting Nyquist diagram for the inertial actuator and passive mount on the rigid base, for the inertial actuator and mount with the initial plate and for one of the inertial actuators in the final arrangement are shown in Figure 5.2.

Figure 5.3 shows disturbance and the predicted level of the error after feedback control with a fixed gain controller for the initial arrangement 5.3(a) and the final experiment 5.3(b).

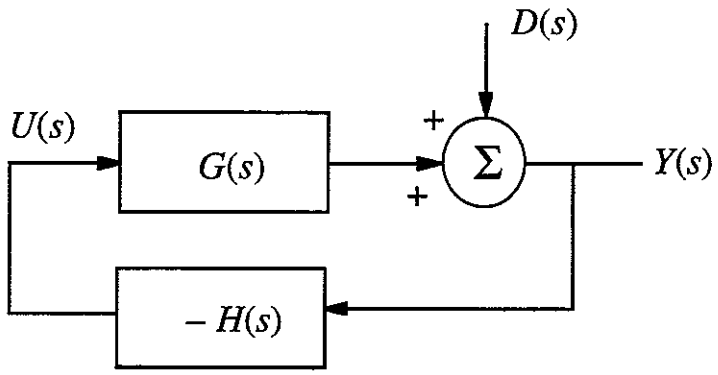

Figure 5.1Block diagram of a single channel feedback controller

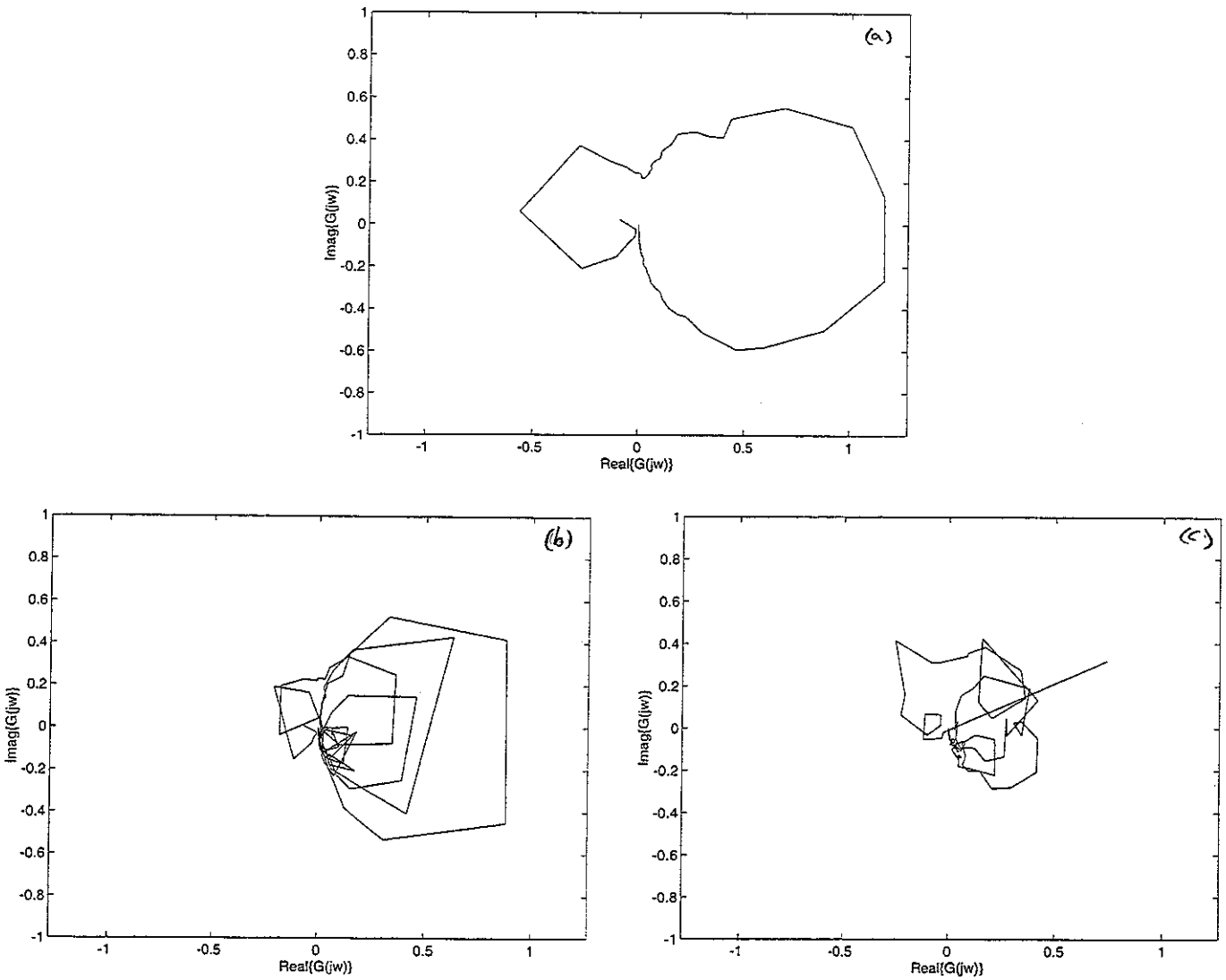

Figure 5.2 Nyquist plots for the open loop control system with a fixed feedback gain for inertial actuator and mount (a) on the rigid base and (b) with the plate in the initial arrangement (c) in the final experiments.

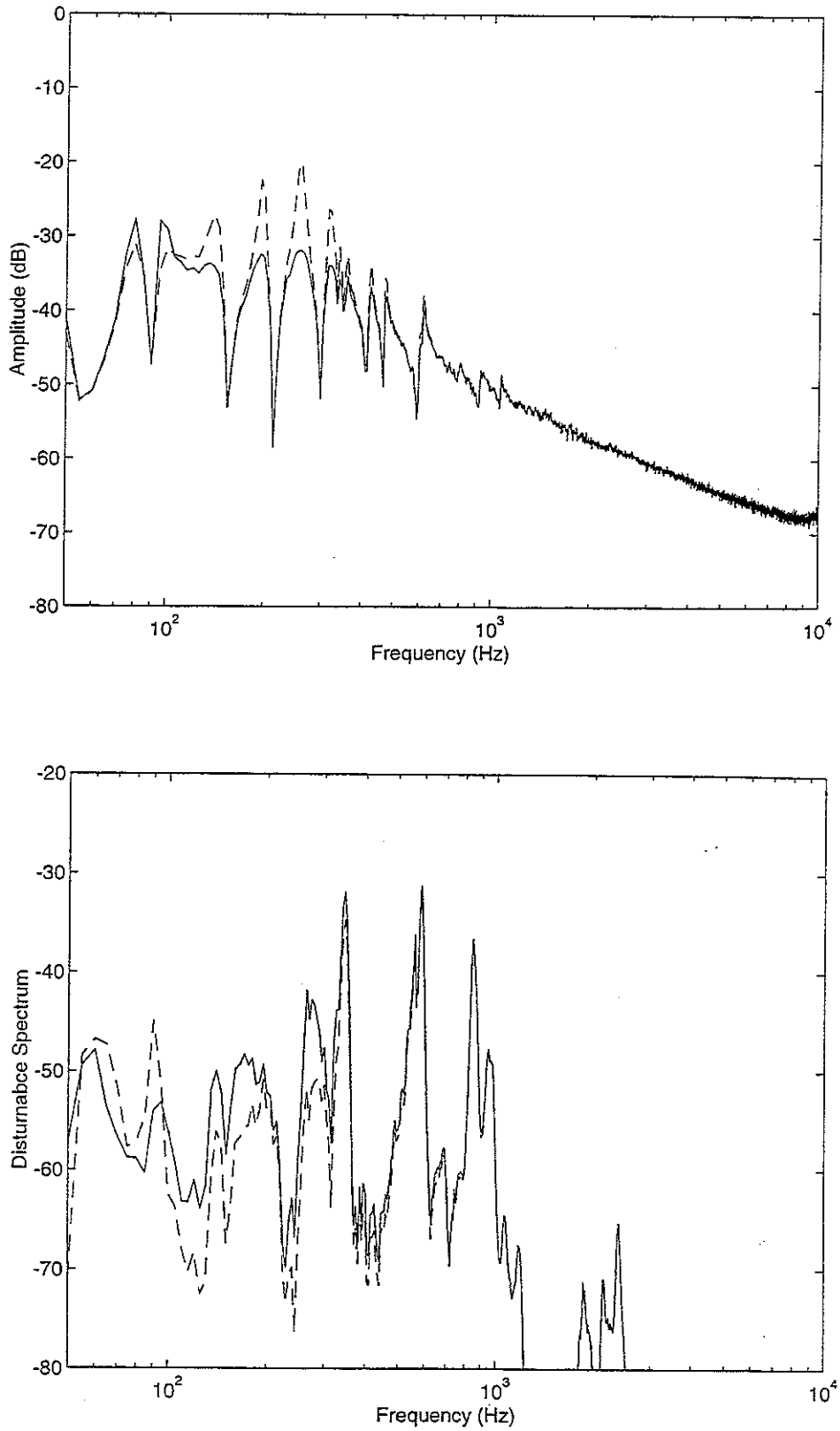

Figure 5.3 *Measured power spectral density of the disturbance at the accelerometer (solid line) and that of the predicted error signal after feedback control (dashed line) for the initial arrangement (a) and the final experiments (b).*

6. EFFECT OF THE ACTUATOR DYNAMICS ON SYSTEM STABILITY

It is clear from the Nyquist plots shown in Figure 5.2 that the main cause of instability as the gain is increased in the feedback loop is the actuator dynamics. In this section we investigate the effect on the stability of changes in the actuator dynamics.

Figure 6.1 shows the frequency response of the two degree of freedom model for the inertial actuator on the passive mount, Figure 3.1, for the mass and stiffness values used above, Figure 6.1(a), and for the same model with half the actuator stiffness ($K_2 = 7.5\ Nmm^{-1}$) but the same viscous damping $C_2 = 10\ Nm^{-1}s$. The effect of halving the actuator stiffness is to reduce the natural frequency of the first resonance, which is mainly associated with the actuator, by about 40%, but not to significantly effect the natural frequency of the second resonance, which is mainly associated with the passive mount.

Because the amplitude as well as the natural frequency of the first resonance has been decreased the gain of the system has been reduced when the phase passes through 180°. When the Nyquist plots of these two systems are plotted, in Figures 6.1(b), the lower actuator resonance thus results in a smaller loop on the left hand side of the imaginary axis. If this modified actuator was incorporated into a simple negative feedback system, the gain could be increased by a further 6 dB compared with the original system before instability, and thus a greater reduction in the disturbance could be achieved.

Instead of changing the stiffness of the suspension inside the actuator, it may be possible to use a compensator circuit to modify the input signal to the actuator to achieve the same result. If the original blocked response of the actuator is

$$T_A(j\omega) = \frac{\omega^2 M}{K - \omega^2 M} \tag{6.1}$$

and the required response is

$$T_A'(j\omega) = \frac{\omega^2 M'}{K' - \omega^2 M'} . \tag{6.2}$$

Then the response of the compensator is equal to

$$C(j\omega) = \frac{T_A'(j\omega)}{T_A(j\omega)} = \frac{M'}{M} \frac{K - \omega^2 M}{K' - \omega^2 M'} . \tag{6.3}$$

In particular if $M' = M$ and $K' = K/2$, as in the example above, then

$$C(j\omega) = \frac{2K - 2\omega^2 M}{K - 2\omega^2 M} = \frac{2\omega_o^2 - 2\omega^2}{\omega_o^2 - 2\omega^2} . \tag{6.4}$$

If K is assumed complex, as above, so that ω_o is also complex, the frequency response of this compensator is plotted in Figure 6.2. The gain is 2 at low frequencies, to compensate for the change in stiffness, and 1 at higher frequencies, since the motion is then mass-controlled.

Although the compensator is guaranteed to perfectly transform the dynamics of the actuator when mounted on a rigid base, the dynamics are more complicated when the actuator is mounted on the flexible mount for example. The physical actuator resonance shifts slightly as a result of mounting on a compliant system and so the use of the compensator derived above will not just transform the actuator natural frequency but results in the more complicated dynamics shown in Figure 6.3. The gain margin of the controller has still been considerably increased by the use of the compensator, but now appears to be quite sensitive to small extraneous phase shifts.

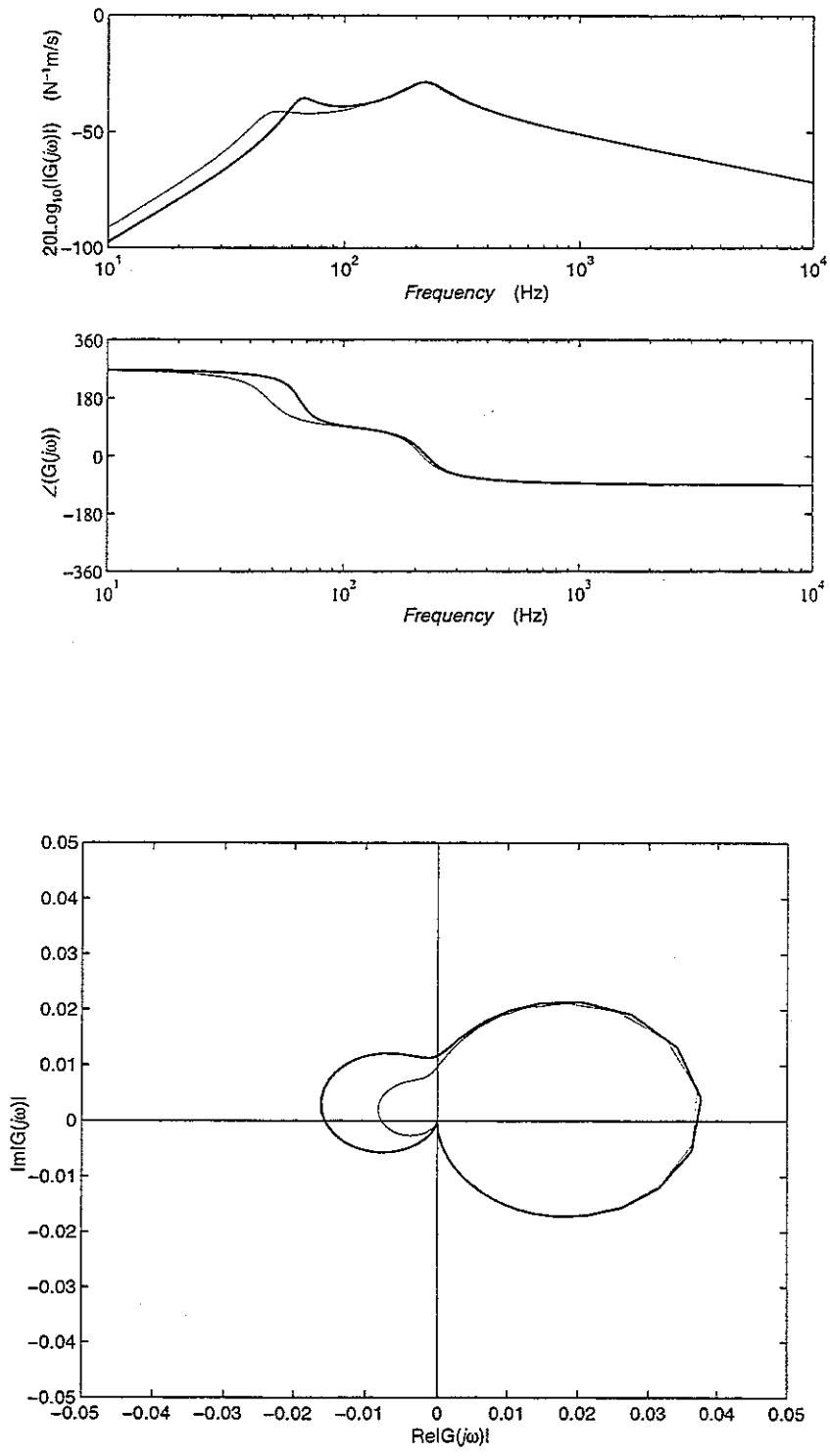

Figure 6.1. Frequency responses of the two degree of freedom model of the internal actuator on the passive mount with the original parameters (solid line) and with half the actuator stiffness (faint line), together with the Nyquist plots of the original (solid line) and modified (faint line) responses.

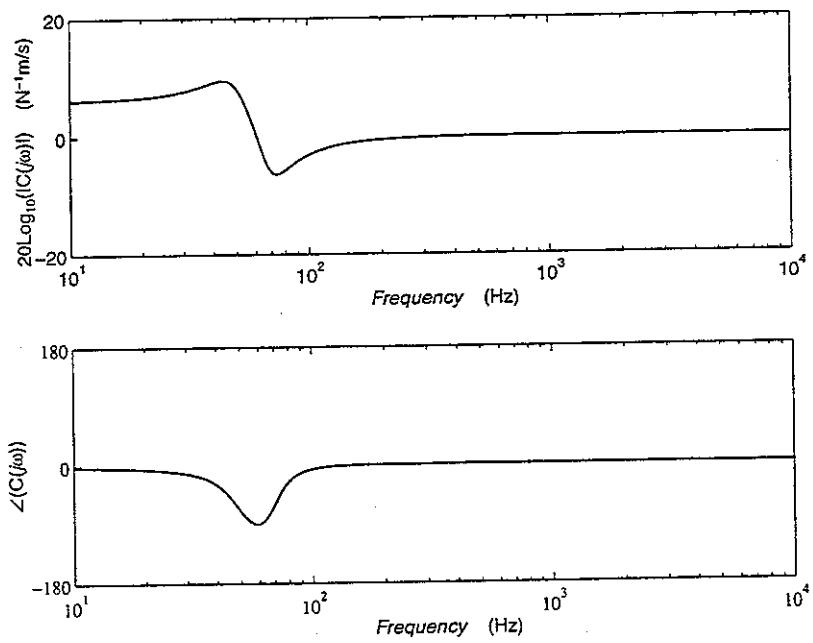

Figure 6.2 Frequency response of the compensator circuit which would make the inertial actuator appear to have half the original suspension stiffness.

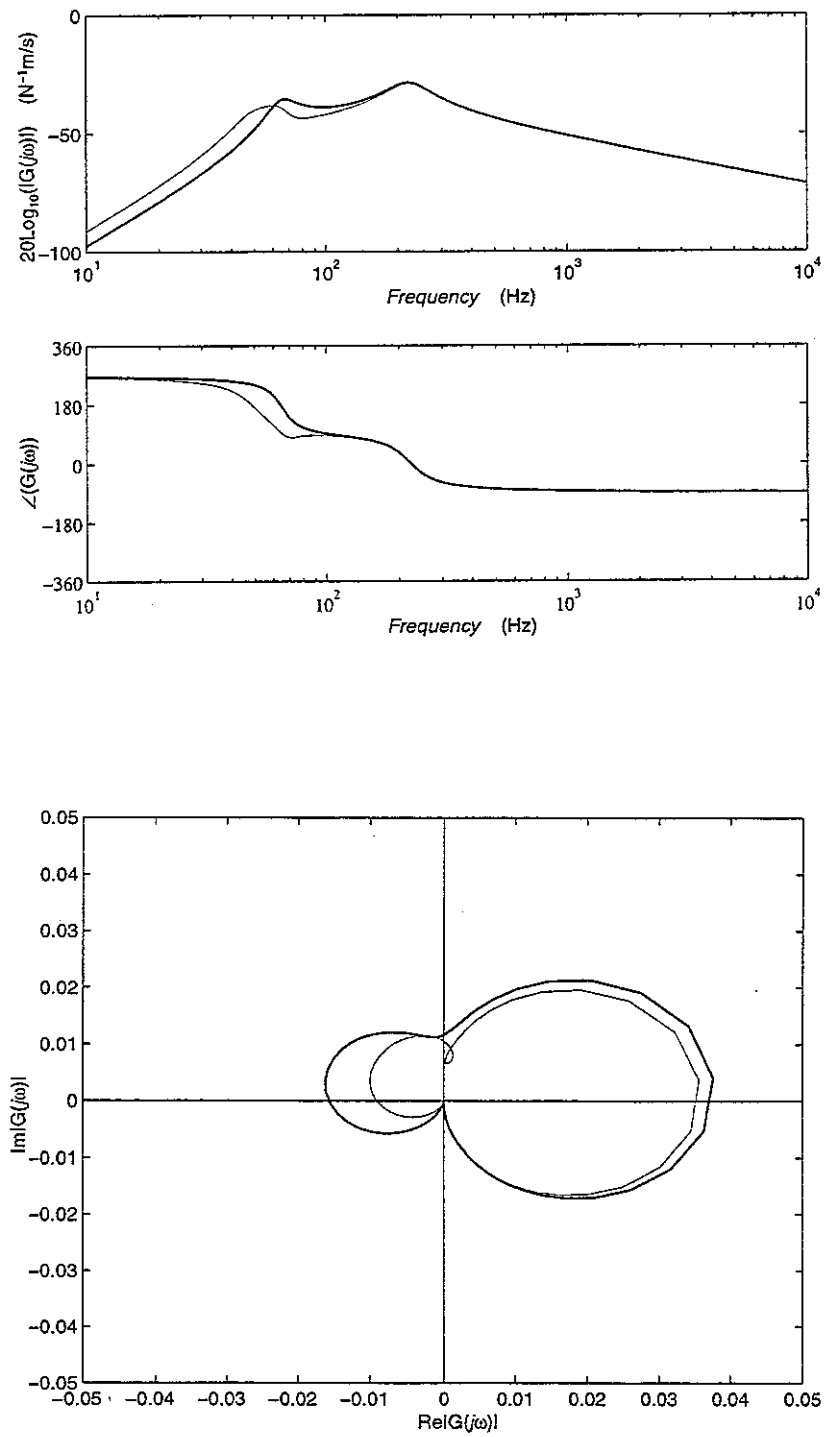

Figure 6.3 Frequency response of the two degree of freedom model of the inertial actuator on the passive mount (solid line) and after multiplication with the compensator shown in Figure 6.2 (faint line) together with the corresponding Nyquist plots.

7. MULTICHANNEL FEEDBACK CONTROLLER

The block diagram of a multichannel feedback controller is shown in Figure 7.1. The vector of output signals $\mathbf{e}(s)$ is related to the vector of disturbances, $\mathbf{d}(s)$, by the sensitivity matrix $[\mathbf{I}+\mathbf{G}(s)\mathbf{H}(s)]^{-1}$ so that

$$\mathbf{e}(s) = [\mathbf{I}+\mathbf{G}(s)\mathbf{H}(s)]^{-1}\mathbf{d}(s) . \tag{7.1}$$

The stability of the multichannel feedback system is determined by whether the roots of the characteristic equation which is given by

$$\det[\mathbf{I}+\mathbf{G}(s)\mathbf{H}(s)] = 0 \tag{7.2}$$

lie in the right hand half of the s plane. The multichannel equivalent to the Nyquist criterion on the open loop frequency response is that the locus of the complex function given by

$$\det[\mathbf{I}+\mathbf{G}(j\omega)\mathbf{H}(j\omega)] = 0 \tag{7.3}$$

encloses the Nyquist point as ω varies from $-\infty$ to ∞. This plot is rather difficult to interpret and so we can use the fact that the determinant of a matrix is the product of its eigenvalues to show that

$$\det[\mathbf{I}+\mathbf{G}(j\omega)\mathbf{H}(j\omega)] = (1+\lambda_1(j\omega))(1+\lambda_2(j\omega))\cdots \tag{7.4}$$

where $\lambda_1(j\omega)\lambda_2(j\omega)$, etc, are the frequency dependent eigenvalues of $\mathbf{G}(j\omega)\,\mathbf{H}(j\omega)$. For the complete system to be stable the Nyquist plot of each $\lambda_i(j\omega)$, the characteristic loci, must not encircle the Nyquist point as ω varies from $-\infty$ to ∞ (Skogestad and Postlethwaite, 1996).

If perfect inertial actuators were used, which generated a constant force per unit input at all frequencies, together with perfectly collocated velocity sensors, then the matrix of plant response, **G**, would be directly proportional to the matrix of input mobilities to the structure under control. If we also assume decentralised control, i.e. independent local control of each loop, with equal feedback gains, then the matrix of feedback controllers **H** is equal to the feedback gain multiplied by the identity matrix, so that under these conditions

$$\mathbf{G}(j\omega)\mathbf{H}(j\omega) \,\alpha\, \mathbf{M}(j\omega) \tag{7.5}$$

where $\mathbf{M}(j\omega)$ is the input mobility matrix.

The mechanical power supplied to the system can be written at a single frequency as a function of the vector of complex forces $\mathbf{f}(j\omega)$ and the vector of complex velocities at the connection points, $\mathbf{v}(j\omega)$, as

$$W = \tfrac{1}{2}\mathrm{Re}\left[\mathbf{f}^H(j\omega)\mathbf{v}(j\omega)\right] . \tag{7.6}$$

But since the velocities are related to the forces via the mobility matrix

$$\mathbf{v}(j\omega) = \mathbf{M}(j\omega)\mathbf{f}(j\omega) , \tag{7.7}$$

then the power can be written as

$$W = \tfrac{1}{2}\mathrm{Re}\left[\mathbf{f}^H(j\omega)\mathbf{M}(j\omega)\mathbf{f}(j\omega)\right] = \mathbf{f}^H(j\omega)\mathbf{R}(j\omega)\mathbf{f}(j\omega) \tag{7.8}$$

where $\mathbf{R}(j\omega)$ is half the real part of $\mathbf{M}(\omega)$. Since power can only be supplied to a mechanical system, W must be positive for all $\mathbf{f}(\omega)$ and so $\mathbf{R}(\omega)$ must be positive definite for all ω.

Because the mobility matrix $\mathbf{M}(j\omega)$ is symmetric then it has an eigenvalue/eigenvector decomposition of the form

$$\mathbf{M} = \mathbf{Q}\,\Lambda\,\mathbf{Q}^{H}. \tag{7.9}$$

If the mobility matrix is split into its real and imaginary parts,

$$\mathbf{M} = \mathbf{R} + j\,\mathbf{X} \tag{7.10}$$

then

$$\Lambda = \mathbf{Q}^{H}\mathbf{R}\mathbf{Q} + j\,\mathbf{Q}^{H}\mathbf{X}\mathbf{Q} \tag{7.11}$$

and if $\mathbf{R}$ is positive definite then so is the diagonal matrix $\mathbf{Q}^{H}\,\mathbf{R}\,\mathbf{Q}$, so that the eigenvalues of $\mathbf{M}$ have a real component which is strictly positive real. The mobility matrix, $\mathbf{M}(\omega)$, can thus be described as strictly positive real (SPR) for all ω.

The locus of the eigenvalues for a 3×3 input mobility matrix calculated for an arrangement similar to that used in the experiments is shown in Figure 7.2 by way of example. Each of these complex eigenvalues are entirely on the right hand side of the imaginary axis for all frequencies, confirming that the mobility matrix is SPR. If independent control is applied from each velocity output to each force input, so that the matrix of feedback controllers is equal to

$$\mathbf{H}(j\omega) = k\,\mathbf{I}, \tag{7.11}$$

then the polar plots for the eigenvalues of the open loop frequency responses will also be SPR. The feedback gain can thus, in principle, be increased without limit without the system becoming unstable. Balas (1979) showed that this was always true provided $\mathbf{H}(j\omega)$ was frequency independent, symmetric and positive semi-definite.

Thus for collocated force actuators and velocity sensors which have a perfect frequency response, simple decentralised control is guaranteed to be stable for any feedback gain and the disturbance at each sensor can, in principle, be reduced to zero using a high gain controller. In practice the dynamic behaviour of the transducer, particularly that of the actuator, limits the maximum feedback gain by introducing additional phase lags into the open loop frequency response, as we have seen for the single channel system above.

The modulus of the measured frequency responses from each inertial actuator to each velocity output are shown in Figure 7.3(a). Notice that above the natural frequencies of the passive mounts, about 300 Hz, the off-diagonal terms in the matrix of plant responses have a progressively smaller value compared with the diagonal terms, which indicates that the transfer mobility on the plate is much less than the input mobility. There is also a much larger phase lag in the off diagonal terms, as shown in Figure 7.3(b), which is also to be expected.

If only one of the velocity signals was fed back to the corresponding actuator the control system could be designed using the single channel approach outlined above. The results of such a design calculated independently for each actuator and sensor pair are shown in Figure 7.4. This shows both the Nyquist plots of the diagonal terms in the plant matrix and the predicted result on the power spectral density of the disturbance signal of a fixed gain feedback controller. It is important to note that the attenuations shown in the individual disturbance spectra in Figure 7.4 could NOT be achieved simultaneously since it has been assumed that only one feedback loop has

been closed at any one time. Although reductions in the disturbance spectra are observed at the error sensor which is being controlled, the disturbance at other error sensors may then be significantly increased.

In order to predict the effect of simultaneously controlling all three channels of the system, the multichannel approach outlined above must be used. Figure 7.5 shows the Nyquist plots of the eigenvalues of the matrix of plant response which are equal to the eigenvalues of the open loop frequency response if the feedback control matrix is diagonal. It was found that reasonable control of all channels could be obtained with a diagonal feedback controller having the gains

$$\mathbf{H}(j\omega) = \begin{bmatrix} 60 & 0 & 0 \\ 0 & 20 & 0 \\ 0 & 0 & 60 \end{bmatrix}. \tag{7.12}$$

The predicted changes in the power spectral densities of each of the disturbance spectra of simultaneously applying such a feedback controller to each channel are also shown in Figure 7.5. The primary disturbances are assumed to be generated by the primary force generating a white noise input. The vector of velocity spectra without control, which correspond to the disturbances above are thus

$$\mathbf{d} = \mathbf{t} f_p \tag{7.13}$$

where f_p is the primary force spectrum and $\mathbf{t}$ is the vector of measured frequency responses between the primary forces and the velocity signals.

The spectral density matrix for the disturbance is thus

$$\mathbf{S}_{dd}(j\omega) = E\left[\mathbf{d}\mathbf{d}^H\right] = \mathbf{t}\mathbf{t}^H \tag{7.14}$$

where it has been assumed that f_p is white and of unit variance so that $E\left[f_p^* f_p\right]=1$. The spectral density matrix for the vector of error signals after control is

$$\mathbf{S}_{ee}(j\omega) \;=\; E\left[\mathbf{e}\mathbf{e}^H\right]. \tag{7.15}$$

The error signals are related to the disturbances via the sensitivity matrix, equation (7.1), so that

$$\mathbf{S}_{ee}(j\omega) \;=\; \left[\mathbf{I}+\mathbf{G}\mathbf{H}\right]^{-1}\mathbf{S}_{dd}\left[\mathbf{I}+\mathbf{G}\mathbf{H}\right]^{-H} \tag{7.16}$$

and since $\mathbf{S}_{dd}(j\omega)$ is given by equation (7.14), $\mathbf{S}_{ee}(j\omega)$ can be calculated entirely from measured frequency responses. The power spectral density of the individual error signals after control are given by the diagonal elements of the matrix $\mathbf{S}_{ee}(j\omega)$ calculated at each frequency.

It can be seen that the results of multichannel control are rather different from those obtained with the independent single channel controllers shown in Figure 7.4, with rather poorer attenuation of the disturbances. It should be emphasised however that the disturbance attenuations shown in Figure 7.5 can now be obtained simultaneously with each feedback loop being closed at the same time.

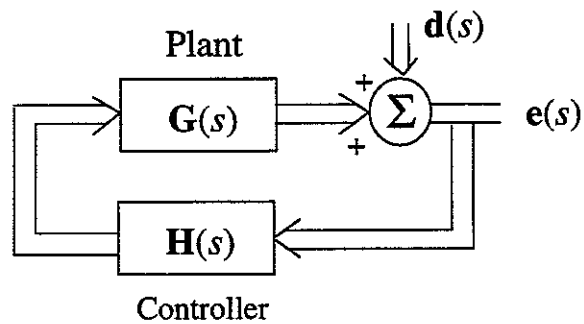

Figure 7.1 Block diagram of multichannel feedback controller.

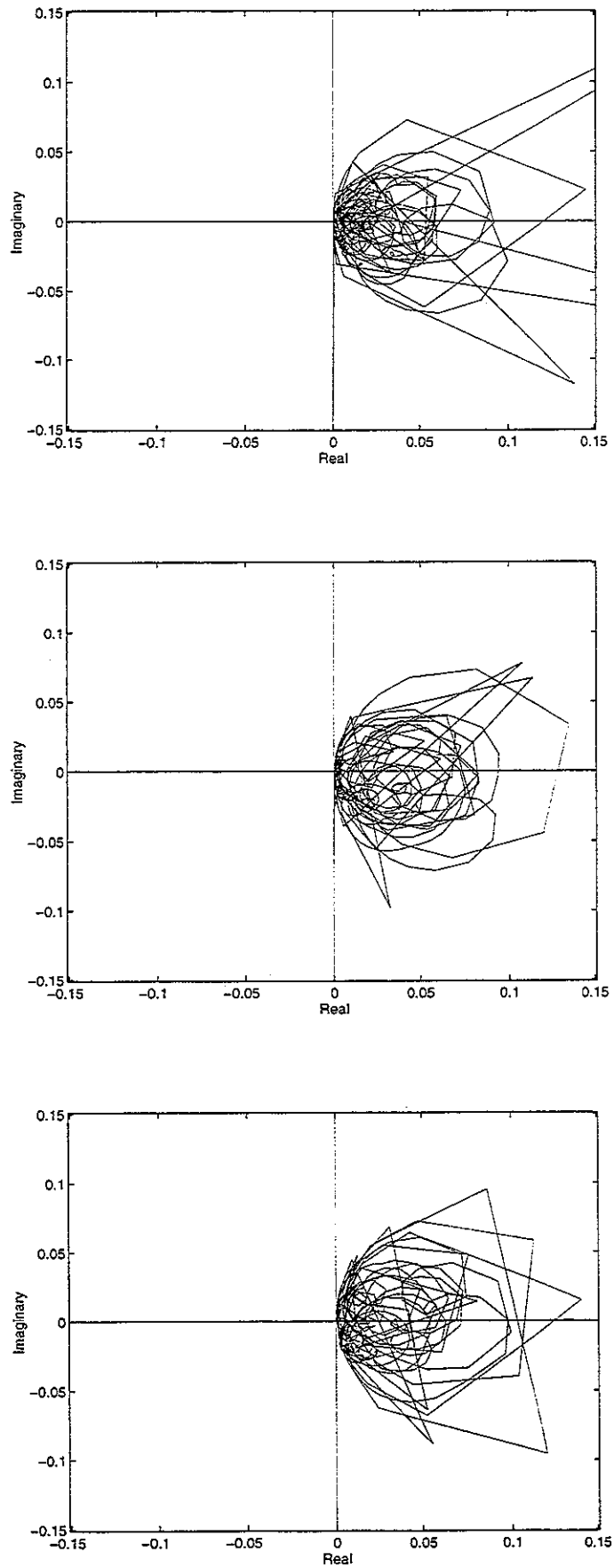

Figure 7.2 Nyquist plots of the eigenvalues of a 3×3mobility matrix calculated for collocated velocity sensors and force actuators. Since the real part of each eigenvalue is always positive, the mobility matrix is said to be strictly positive real (SPR).

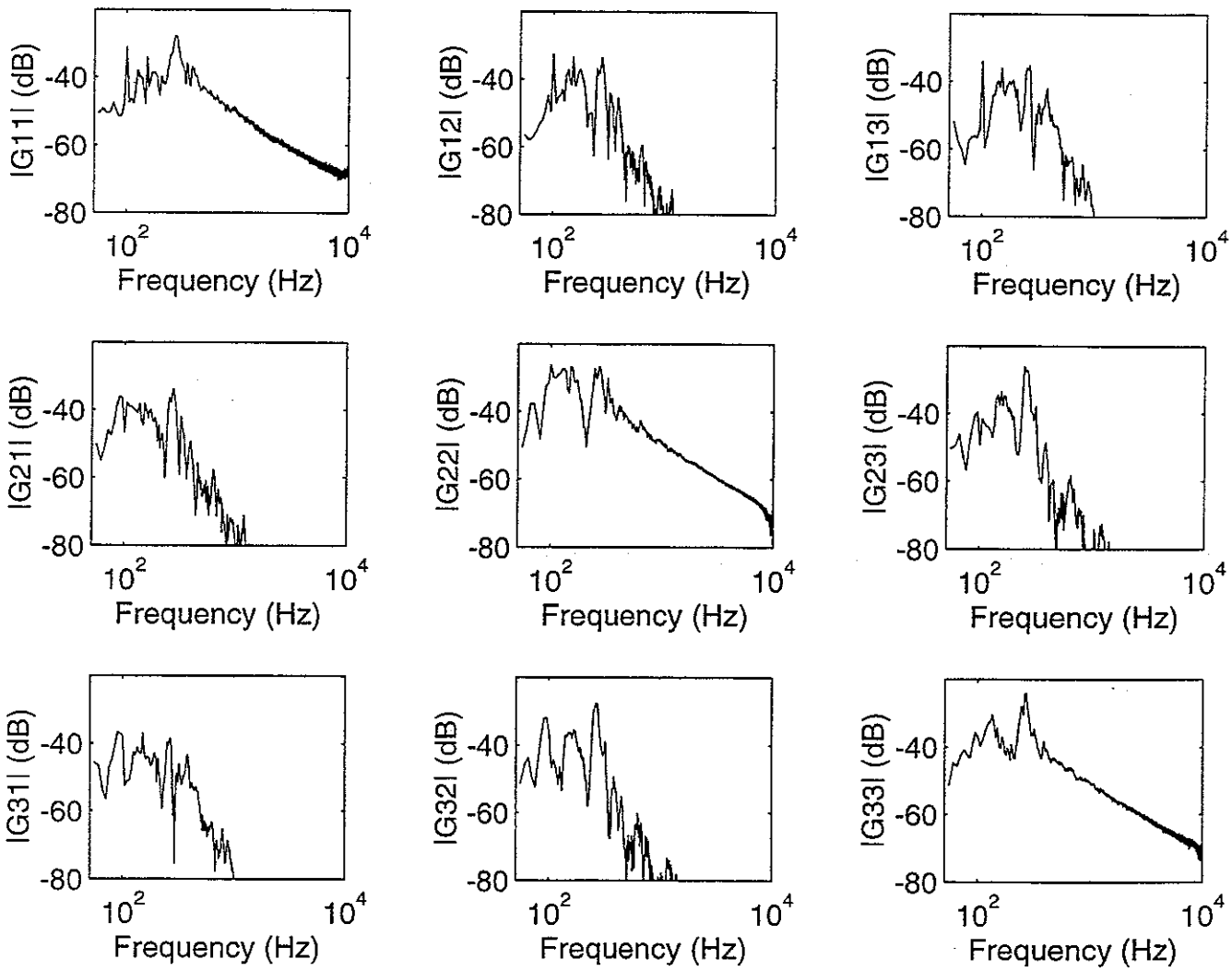

Figure 7.3a The modulus of the frequency responses measured from each actuator to each sensor for the experimental arrangement shown in Figure 4.1.

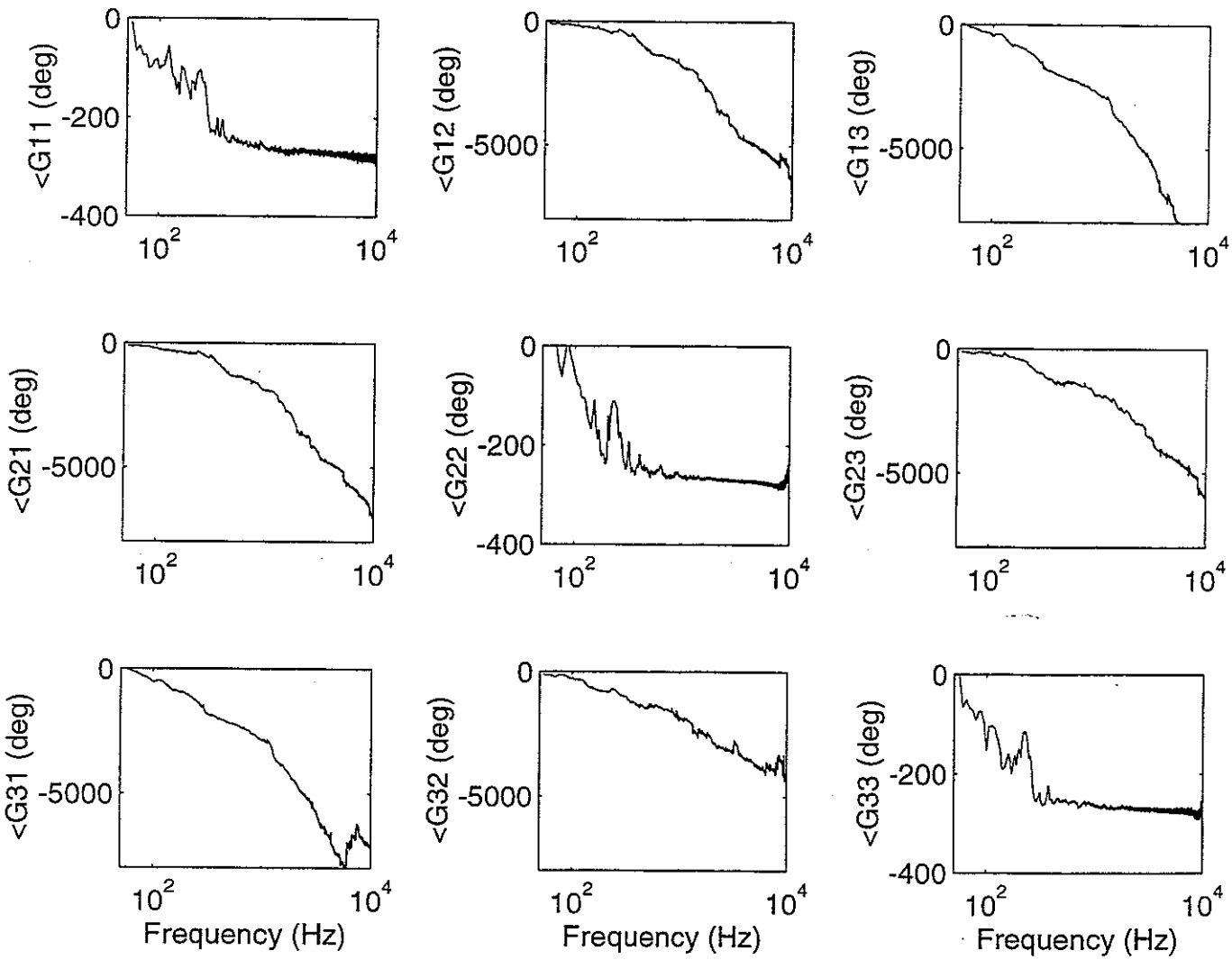

Figure 7.3b The phase of the frequency responses measured from each actuator to each sensor for the experimental arrangement shown in Figure 4.1.

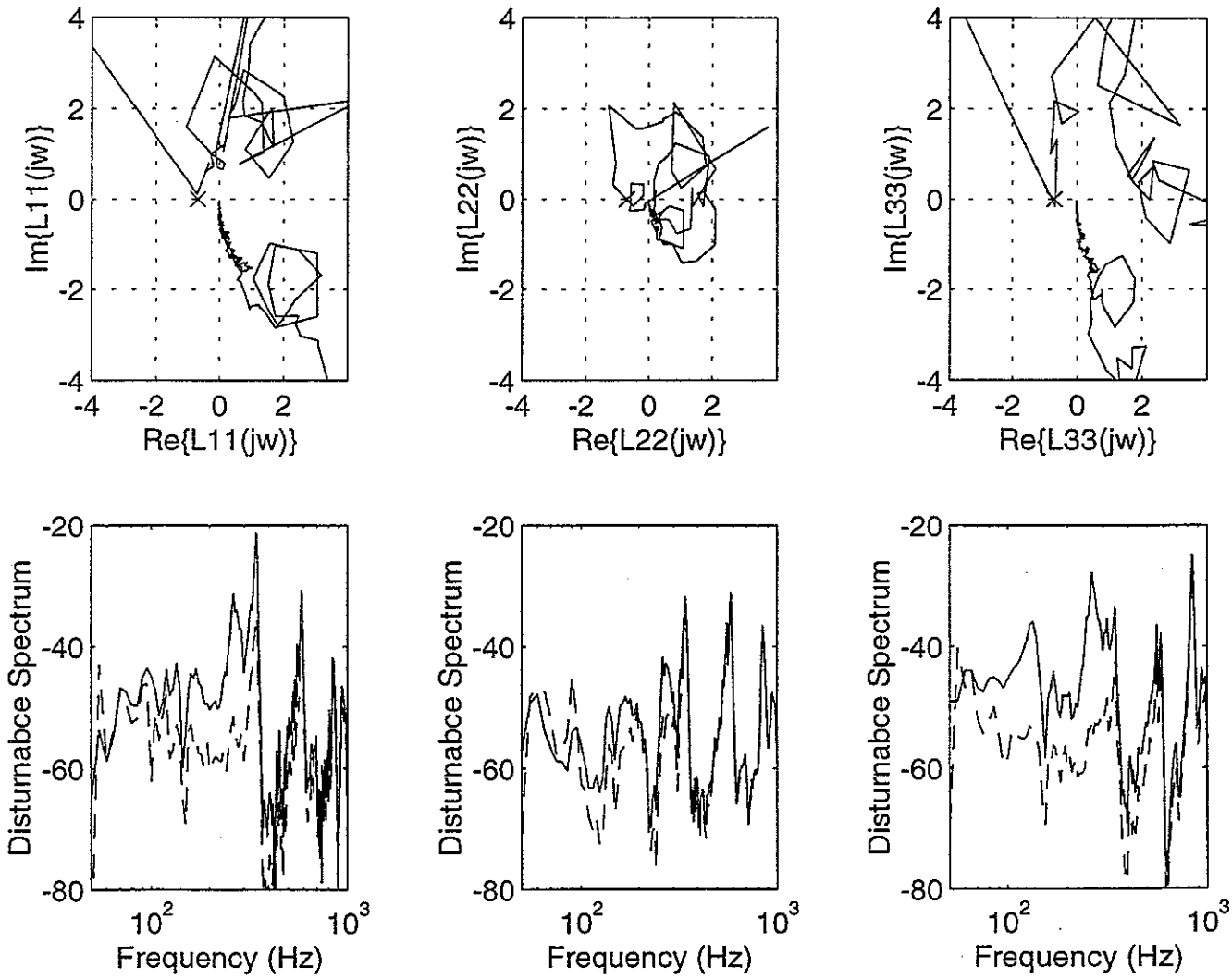

Figure 7.4 The Nyquist plots of the diagonal terms in the matrix of plant responses (upper curves) and the predicted changes in the disturbance spectra if a single channel control system were implemented ***one at a time*** *round each actuator and sensor.*

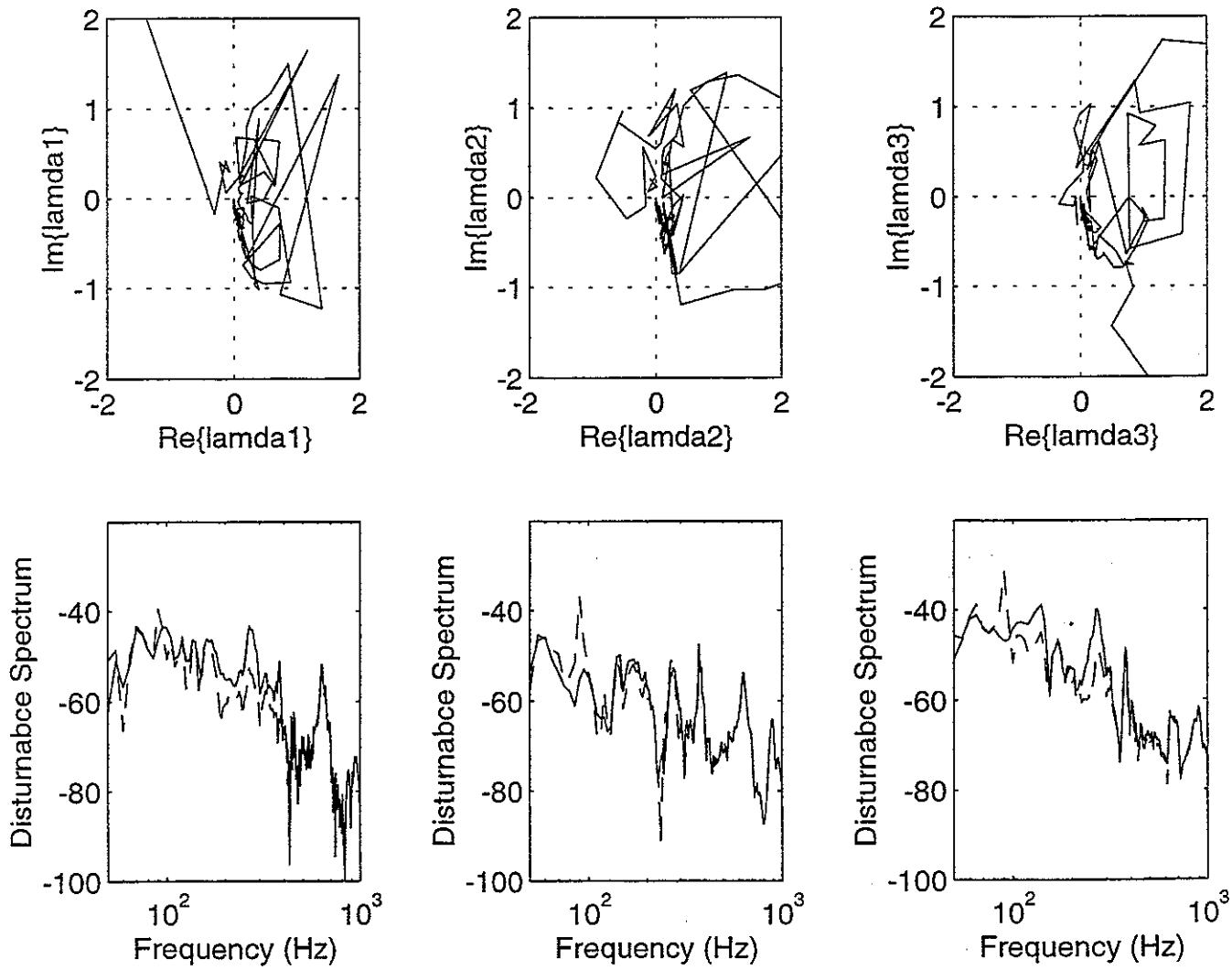

Figure 7.5 The Nyquist plots of the eigenvalues of the matrix of plant responses (upper curves) and the predicted change in the disturbance spectra if a three single channel control system were implemented ***simultaneously*** *round each actuator and sensor.*

8. CONCLUSIONS AND RECOMMENDATIONS FOR FURTHER WORK

A simple model has been developed for the inertial actuator used in the active isolation experiments discussed here. This simple model has been used to predict the main features of the frequency response from the actuator input to velocity output when the actuator is attached to a passive mount, and when the actuator is used in the final experimental arrangement.

The performance of a simple negative feedback controller has been found to be limited by a potential instability caused by the low frequency phase shift of the inertial actuator. The performance could be improved by lowering the suspension stiffness of the actuator or, in principle, by using an electrical compensating circuit, which would allow the gain in the feedback loop to be increased.

In a multichannel feedback system interaction between the individual feedback loops can destabilise the system. It is shown that if collocated force actuators and velocity sensors, which had no internal dynamics, were used in a multichannel controller, the system would be inherently stable, since the real parts of the eigenvalues of the open loop response are strictly positive real (SPR). Once again, however, the actuator dynamics limit the performance by destabilising the system if the feedback gain is too large. The performance of the multichannel controller has been predicted and is rather poorer than that of the individual single channel controller, implemented one at a time. Unfortunately, no measured performance data is available for the change in the velocity signals at the multiple actuator locations when implementing multichannel control to validate these predictions.

Because the predicted vibration performance of the multichannel feedback controller is not as good as the individual single channel controllers and because no experimental validation of these results is available it is recommended that a further

laboratory study be carried out of the three-mount system. This need not be mounted in the reverberation chambers, but since the measured and predicted behaviour will need to be compared repeatedly, it is suggested that these tests are carried out at ISVR. Specifically these measurements would address:

1) The reasons for the differences in the single channel performance between the inner and outer actuators.

2) The variation in the plant response due to changes in the dynamic loading conditions, which would define the multichannel plant "uncertainty" in the system.

3) The optimum design of the individual controllers used in the multichannel system.

4) The comparison of the predicted velocity attenuation in the multichannel system with that measured using a real-time controller.

References

Franklin G.F., Powell J.D. and Emani-Naeini A. (1994) *Feedback control of dynamic systems* (3rd Edition, Addison-Wesley).

Balas M.J. (1979) Direct velocity feedback control of large space structures. *Journal of Guidance and Control*, 2, 252-253.

Skogestad S. and Postlethwaite I. (1996) *Multivariable Feedback Control : Analysis and Design*. John Wiley and Sons.